Oxazolone Versus Macrocycle Structures for Leu-Enkephalin b_2-b_4: Insights from Infrared Multiple-Photon Dissociation Spectroscopy and Gas-Phase Hydrogen/Deuterium Exchange

Xian Chen,[a] Jeffrey D. Steill,[b] Jos Oomens,[b,c] and Nick C. Polfer[a]

[a] Department of Chemistry, University of Florida, Gainesville, Florida, USA
[b] FOM Institute for Plasma Physics Rijnhuizen, Nieuwegein, The Netherlands
[c] University of Amsterdam, Amsterdam, The Netherlands

The collision-induced dissociation (CID) products b_2-b_4 from Leu-enkephalin are examined with infrared multiple-photon dissociation (IR-MPD) spectroscopy and gas-phase hydrogen/deuterium exchange (HDX). Infrared spectroscopy reveals that b_2 exclusively adopts oxazolone structures, protonated at the N-terminus and at the oxazolone ring N, based on the presence and absence of diagnostic infrared vibrations. This is correlated with the presence of a single HDX rate. For the larger b_3 and b_4, the IR-MPD measurements display diagnostic bands compatible with a mixture of oxazolone and macrocycle structures. This result is supported by HDX experiments, which show a bimodal distribution in the HDX spectra and two distinct rates in the HDX kinetic fitting. The kinetic fitting of the HDX data is employed to derive the relative abundances of macrocycle and oxazolone structures for b_3 and b_4, using a procedure recently implemented by our group for a series of oligoglycine b fragments (Chen et al. *J. Am. Chem. Soc.* **2009,** *131*(51), 18272–18282. doi: 10.1021/ja9030837). In analogy to that study, the results suggest that the relative abundance of the macrocycle structure increases as a function of b fragment size, going from 0% for b_2 to ~6% for b_3, and culminating in 31% for b_4. Nonetheless, there are also surprising differences between both studies, both in the exchange kinetics and the propensity in forming macrocycle structures. This indicates that the chemistry of "head-to-tail" cyclization depends on subtle differences in the sequence as well as the size of the b fragment. (J Am Soc Mass Spectrom 2010, 21, 1313–1321) © 2010 American Society for Mass Spectrometry

The central theme in proteomics is to identify the structures and functions of proteins in living systems. Since the emergence of two soft ionization methods, electrospray ionization (ESI) [1, 2] and matrix-assisted laser desorption/ionization (MALDI) [3–5], in the late 1980s, mass spectrometry has become a key technique in the field of proteomics. To obtain sequence information of peptides and proteins, ions are most commonly subjected to ion activation and dissociation by collision-induced dissociation (CID). In low-energy CID, bond breakage mostly occurs at the amide bonds, as this is typically the lowest-energy dissociation pathway. This leads to b ions when the charge is retained by the N-terminal fragment, or y ions when it is retained by the C-terminal fragment [6, 7].

Many mechanistic studies have been carried out over the years to get insights into different aspects of the dissociation chemistry. The role of basic sites in sequestering protons, as well as the role of the "mobile" proton in weakening the amide bond are well-documented [8–10]. Another mechanistic aspect concerns the structure of fragments ions, and b ions in particular [11]. Since the C-terminal carbonyl group in a b ion must be stabilized, Harrison and coworkers proposed that a nucleophilic attack takes place from another backbone carbonyl, resulting in a terminal five-membered ring oxazolone structure [12]. Nonetheless, peptides often exhibit a number of nucleophilic sites, including side-chain groups and the N-terminal amine group [10, 13–16]. In terms of sequencing, it is particularly troublesome if the N-terminus engages in a "head-to-tail" cyclization, giving rise to a macrocycle structure. Harrison and Paizs demonstrated this for the example of the b_5 fragment of the pentapeptide YAGFL-NH_2 [17]. In the proposed reaction scheme, oxazolone and macrocycle structures can freely interconvert, leading to oxazolone structures with permuted sequences, which then give rise to nondirect sequence ions. Unusual dissociation processes had been reported by others previously. Boyd and coworkers reported one of the first observations of gas-phase rearrangement reactions in CID [18, 19]. Such rearrangement processes were also

Address reprint requests to Dr. N. Polfer, Department of Chemistry, University of Florida, P.O. Box 117200, Gainesville, FL 32611-7200, USA. E-mail: polfer@chem.ufl.edu

1044-0305/10/$32.00
doi:10.1016/j.jasms.2010.02.022

Published online February 18, 2010
Received December 15, 2009
Revised February 11, 2010
Accepted February 11, 2010

seen for an a-type fragment in YGGFL by Vachet and Glish [20].

The first direct evidence for a mixture of oxazolone and macrocycle structures comes from infrared multiple-photon dissociation (IR-MPD) spectroscopy by Polfer et al. on b_4 generated from YGGFL [21]. Oxazolone and macrocycle structures are identified based on diagnostic vibrations involving the oxazolone ring C = O stretch and macrocycle CO-H^+ bending. A number of b_2 fragments have been characterized to date with this technique in studies by Wysocki [22], Oomens [23], Paizs and coworkers [23], all exhibiting oxazolone structures. Recently, however, a study by Wysocki has shown that cyclic diketopiperazine b_2 structures are formed for the sequence His-Ala [24]. Studies on larger b fragments appear to show a higher prevalence for forming macrocycle structures. Maitre and coworkers showed that the b_5 fragment of GGGGGR exclusively gives rise to macrocycle structures [25]. Chen et al. observed that for a series of oligoglycine b fragments, the smaller b_2 and b_3 exclusively adopt oxazolone structures, whereas mid-sized fragments (b_4-b_7) exhibit a mixture of oxazolone and macrocycle structures. For b_8, exclusively macrocycle structures were seen, clearly showing an effect of the fragment size on oxazolone versus macrocycle formation. While IR-MPD spectroscopy was crucial in identifying the structures formed, Chen et al. employed gas-phase hydrogen/deuterium exchange (HDX) to quantify the relative amounts of the chemical structures that were formed. This quantification was based on differences in HDX kinetics between oxazolone ("fast") and macrocycle ("slow") structures [26].

In earlier studies, Wysocki and Somogyi had shown that HDX of b ions often displays bimodal distributions, which can be rationalized by the presence of two different chemical structures [27, 28]. Recent HDX studies by Solouki and coworkers also show similar trends [29]. HDX presents substantial advantages in that the technique is easy to implement in trapping mass spectrometers, and that the relative amounts of the products can be quantified based on the kinetic data [26, 29]. Note that such a quantification is also achievable in principle by ion mobility mass spectrometry, even if full separation is not always possible, as shown in studies by Garcia and Gaskell on b_5 from YAGFL-NH_2 [30, 31], as well as measurements on a_4 and b_4 from YGGFL by Polfer et al. [32]. Despite the ease of implementation of HDX, the structural interpretation of such studies is often ambiguous, due to an incomplete understanding of the HDX mechanism.

The combined approach of IR-MPD spectroscopy and gas-phase HDX is hence well-suited to this problem, as recently shown by our group [26]. We apply this complementary methodology here to study the b_2-b_4 CID products of Leu-enkephalin. Both techniques are highly complementary, as they cancel out each others' weaknesses. While IR-MPD spectroscopy confirms the chemical structures that are formed, HDX allows their quantification.

Experimental

Sample Preparation

The pentapeptide Leu-enkephalin (Tyr-Gly-Gly-Phe-Leu) (Sigma Aldrich, St. Louis, MO, USA) and deuterating reagent CH_3OD (Sigma Aldrich) were employed without further purification. Leu-enkephalin was used as 20 μM solution in 50:50 water/methanol with 2% acetic acid to aid protonation.

Mass Spectrometry and Hydrogen/Deuterium Exchange

The hydrogen/deuterium exchange (HDX) experiments were carried out at the University of Florida using a commercially available 4.7 Tesla actively shielded Bruker Bioapex II Fourier transform ion cyclotron resonance (FT-ICR) mass spectrometer equipped with an Apollo API 100 source (Bruker Daltonics, Billerica, MA, USA), as reported in our recent publication [26]. The singly protonated Leu-enkephalin (*m/z* 556) was ionized by electrospray ionization (ESI). "Nozzle-skimmer" dissociation was applied in the ESI source region by adjusting the voltage drop between the metal-plated glass capillary and the first skimmer to activate the protonated peptide precursor. The CID product ions were then accumulated in the hexapole for 3s, before transfer to the ICR cell. A frequency sweep was performed in the FT-ICR experimental sequence to eject other ions and to mass-isolate each desired b product ion (b_2-b_4). The monoisotopic peak of each species was then subjected to gas-phase hydrogen/deuterium exchange (HDX) with CH_3OD in the ICR cell for different time periods. CH_3OD was leaked into the vacuum chamber using a Varian leak valve (Varian, Mountain View, CA) to attain a constant pressure of 1×10^{-8} Torr. Note that CH_3OD was degassed using several freeze-thaw cycles before introduction into the mass spectrometer.

Mass spectra with different HDX times were recorded, and the abundances for the undeuterated (d_0), singly deuterated (d_1), etc. peaks in the resulting distributions were determined. The data are represented here by plotting the natural logarithm of the ratio of d_0 divided by the sum of all ions, $\ln[d_0/\Sigma d_n]$, as a function of the HDX time, as described previously [26]. The depletion of d_0 is also represented as a percentage, which is plotted on a natural logarithm scale. Because the exchange reagent is considered to be in great excess of the analyte, the H/D exchange reaction can be approximated as a first-order reaction in the analyte concentration. Linear fits were performed to determine the reaction kinetics.

Mass Spectrometry and Infrared Photodissociation Spectroscopy

The infrared photodissociation experiments were performed at the FOM Institute for Plasma Physics Rijnhuizen using the free electron laser FELIX [33]. A laboratory-built FT-ICR mass spectrometer described in detail previously [34, 35] was employed for the mass spectrometry measurements. The fragment ions (b_2, b_3) were generated by "nozzle-skimmer" dissociation. The infrared spectrum for b_4 is taken from a previously published study [21]. The fragment ion was accumulated in the hexapole, and then transferred to the ICR cell. The ion of interest was mass-selected and irradiated with the tunable output from the free electron laser. FELIX produces macropulses (5 μs) at a repetition rate of 5 Hz. The macropulses consist of a train of micropulses separated by 1 ns. The pulse energy per macropulse is dependent on wavelength, reaching maximum values of 60 mJ at 12 μm, depending on the electron beam energy. Typically, 20–30 macropulses were employed to induce efficient photodissociation.

The IR photodissociation spectrum was recorded by monitoring the infrared multiple-photon dissociation (IR-MPD) yield as a function of the wavelength (here 1300–1975 cm^{-1}). This yield is represented as yield = $-\ln[1 - (\Sigma\text{photofragments}/\Sigma\text{all\_ions})]$. The yield is further normalized linearly with FELIX laser power at each wavelength step. The main photodissociation product of b_3 (*m/z* 278) was found to be *m/z* 221 (b_2), as well as a minor fragment at *m/z* 193 (a_2). For b_2 (*m/z* 221), the *m/z* 193 (a_2) photofragment was most abundant. The theory of the IR-MPD mechanism will not be discussed here, as there have been a number of recent review articles on the fundamental and practical aspects of IR-MPD spectroscopy [36–43].

Computations

Calculations were carried out at the High-Performance Computing (HPC) Center at the University of Florida using the AMBER force field [44] and the Gaussian03 package [45].

Candidate structures for b_2 fragments were generated using an in-house developed method, involving conformational searching by molecular mechanics and frequency calculations by density functional theory (DFT). The chemical structures (oxazolone and diketopiperazine) were initially built and optimized using semi-empirical methods (AM1) in HyperChem (Hypercube Inc., Gainesville, FL, USA). For oxazolones, two proton attachment sites were considered at the N-terminus and oxazolone ring nitrogen. For the diketopiperazine structure, merely the backbone carbonyl oxygen was considered.

The chemical input structures for the molecular mechanics calculations required a parameterization procedure. The AM1 structures were optimized using DFT (B3LYP/6-31G*), followed by an electrostatic potential fitting with ab initio methods (HF/6-31 g*) to derive the atomic point charges. The geometry and ESP-derived charges were imported into the AMBER suite of programs, where a restrained electrostatic potential (RESP) fitting was performed [46]. Each chemical structure was parameterized separately in AMBER, followed by a conformational search using simulated annealing cycles. Two separate runs with starting temperatures at 300 and 500 K were carried out, resulting in 200 candidate structures per dynamics simulation.

All output structures from AMBER were then optimized again at the DFT level, initially using B3LYP/3-21G. Further optimization was performed at the B3LYP/6-31G(d). Merely the 20 unique lowest-energy conformers were then optimized at B3LYP/6-31G+(d,p), followed by a single-point MP2/6-31G+(d,p) calculation. The MP2 electronic energy for each conformer was corrected for the zero-point energy (ZPE) from B3LYP/6-31G+(d,p) of theory to yield the final ZPE-corrected energies. Note that MP2 energies were considered to account for the dispersion interaction involving the tyrosine side-chain. All energies presented here are relative to the lowest-energy conformer (for Hartrees see Table S2, Supporting Information file, which can be found in the electronic version of this article). The frequency spectra of the lowest-energy structures at the B3LYP/6-31G+(d,p) level were scaled by 0.965; this scaling factor was found to be useful in previous IR-MPD spectroscopy studies of peptide fragments [21]. Stick spectra were convoluted using a 20 cm^{-1} full width at half-maximum (FWHM) Gaussian profile to allow easier comparison with the recorded IR photodissociation spectra.

Results and Discussion

Infrared Spectroscopy Results

The b_2 fragment (*m/z* 221), generated by "nozzle-skimmer" CID from protonated Leu-enkephalin, was structurally interrogated by IR-MPD spectroscopy in the mid-IR range (1300–1975 cm^{-1}). This experimental spectrum is compared to a number of chemical structures, including an oxazolone structure protonated on the N-terminus (oxazolone N-prot), an oxazolone structure protonated on the oxazolone ring N (oxazolone ox-prot), and a cyclic diketopiperazine structure protonated on a carbonyl O (diketopiperazine O-prot). Figure 1 displays a comparison of the experimental results with the calculated spectra of the lowest-energy conformer for each chemical structure, along with their structures and relative energies. As explained in the Experimental section, the electronic energies (MP2) are corrected for ZPE at B3LYP/6-31G(d,p). Both stick spectra and convoluted Gaussian profiles are shown for easier comparison. The structures are also shown in a larger format in the Supporting Information (Figure S1).

There is no match between the experimental spectrum and the diagnostic modes of protonated diketopiperazine structure, despite the fact that this struc-

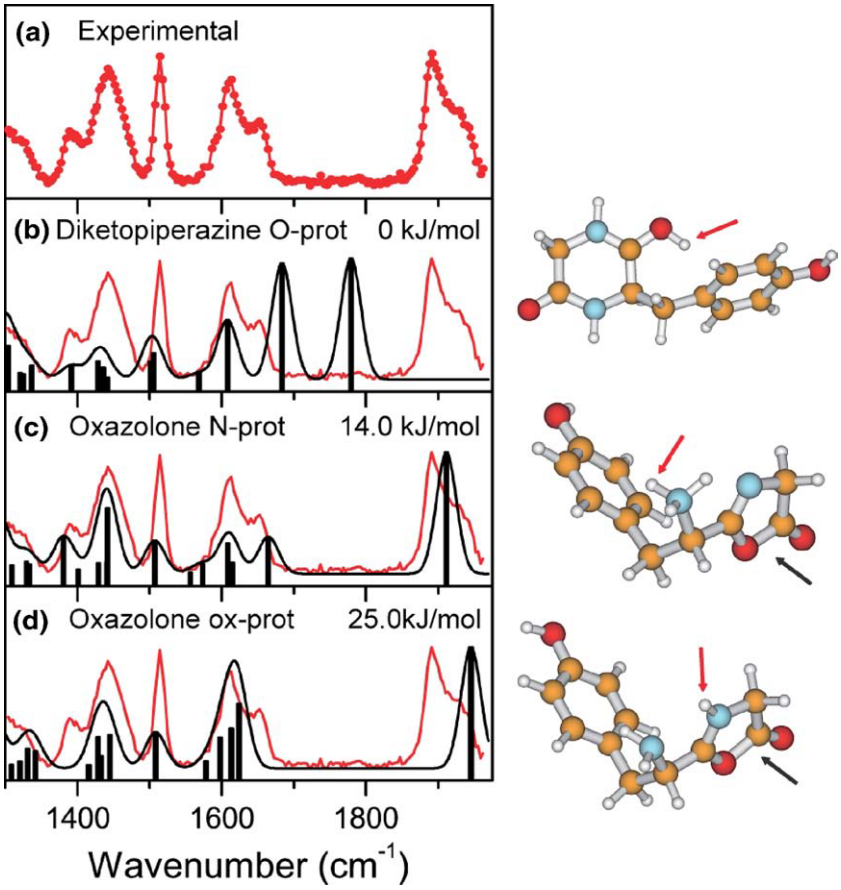

Figure 1. (**a**) IR-MPD spectrum of the b_2 fragment generated from protonated Leu-enkephalin, compared to computed spectra for (**b**) diketopiperazine structure protonated on a carbonyl O, (**c**) oxazolone structure protonated on the on the N-terminus, and (**d**) oxazolone structure protonated on the oxazolone ring N. The scaling factor 0.965. Corresponding structures are presented on the right. The site of proton attachment (red arrow) and oxazolone rings (black arrow) are indicated.

ture is lowest in energy. The prominent C=O (1810 cm^{-1}) and C–N (1715 cm^{-1}) stretches are clearly not observed. Similar results have been observed by others for b_2 fragments in different systems, Ala-Ala by Oomens et al. [23], and Ala-Gly by Wysocki and coworkers [22], Gly-Gly by our group [26], and a number of b_2 fragments from tryptic digest peptides by Maitre and coworkers [25]. This indicates that the kinetic barrier to a nucleophilic attack from the N-terminus is too high, and hence the oxazolone formation pathway is favored for kinetic reasons, as predicted by Paizs [47].

The broad feature around 1900 cm^{-1} clearly shows one main peak and a prominent shoulder, which is consistent with the presence of oxazolone N-prot and ox-prot structures. The lower-frequency peak of that distribution is assigned to the oxazolone C=O stretch of the N-prot structure, whereas the higher-frequency shoulder matches the corresponding band of the oxazolone ox-prot structure. The predicted energy gap, calculated at the MP2 (Møller-Plesset) level (~11 kJ mol^{-1}) is somewhat large to account for the presence of both structures, and hence this may be due to slight inaccuracies in the calculation. Nonetheless, the computations favor the N-prot oxazolone, which also seems to be validated by the significantly more intense band for this structure in the IR-MPD spectrum. This is in strong contrast to the b_2 fragments involving primary structures Gly-Gly [26], Ala-Gly [22], and Ala-Ala [23], where the ox-prot structure mainly accounts for the structures that are observed. The structures confirm that the tyrosine side chain in b_2 YG plays an important role in stabilizing the N-prot oxazolone, due to interaction between the proton and the tyrosine π-cloud. To account for these interactions more accurately, the energies are computed at the MP2 level, which includes dispersion interactions.

The experimental mid-IR-MPD (1300–1975 cm^{-1}) spectra for b_2 (*m/z* 221), b_3 (*m/z* 278), and b_4 (*m/z* 425) are compared in Figure 2. Note that only b_2 and b_3 were recorded in this study, whereas b_4 originates from a previous study by Polfer et al. [21]. Clear differences between the spectra can be seen, which also assist the interpretation. The chemical interpretations of the spectral bands are indicated and are based on comparisons with DFT-calculated spectra for b_2 (this study) and b_4 (see [21]). The bands in the region 1780–1940 cm^{-1} are

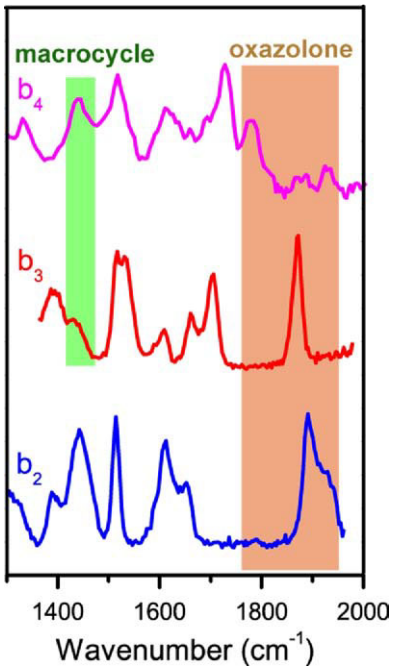

Figure 2. Overlaid mid-IR-MPD spectra of b_2, b_3, and b_4. The spectrum of b_4 is adapted from previous publication of Polfer at al. [21]. The chemically diagnostic modes are indicated.

chemically diagnostic modes for oxazolone C=O stretch modes, as these consistently appear in a higher frequency region than the amide C=O stretch. It can be seen that the position of the oxazolone C=O stretch is progressively red-shifted in larger b fragments, due to an increase in hydrogen-bonding interactions. While b_2 and b_4 exhibit multiple bands, b_3 merely appears to show one band, suggesting that one site of proton attachment is exclusively observed. While no comparison to theory was performed for b_3, it seems likely that N-prot oxazolone is favored, since this is also the case for b_2 and b_4. In terms of macrocycle identification, the macrocycle CO-H^+ bending mode is expected at ~1440 cm^{-1} [21]. This is not a pure mode that is exclusively due to CO–H^+ bending for a proton shared between two carbonyls. In the IR-MPD spectrum of b_2, where such a CO–H^+ bending mode is not possible the band at 1440 cm^{-1} corresponds to CH_2 bending on the oxazolone ring. Nonetheless, the proton bending mode lends brightness to the band at this position. In the previous study by Polfer et al. [21], the IR-MPD spectrum of Leu-enkephalin b_4 was assigned as a mixture of oxazolone and macrocycle structures, due to the prevalence of the band at 1440 cm^{-1}. Here, the corresponding macrocycle band at 1440 cm^{-1} for b_3 is found to be much weaker (compared with b_4). This is consistent with the picture that the relative abundance for macrocycle structures in b_3 is lower than in b_4, if present at all.

In summary, the IR spectra provide strong evidence that b_2 is exclusively composed of oxazolone structures, whereas a mixture of oxazolone and macrocycle structures are observed for b_4. For b_3 the picture is less clear. An oxazolone structure is identified unambiguously, however, the presence of the macrocycle is harder to establish due to the spectral overlap between CO–H^+ bending and oxazolone ring CH_2 bending. The complementary technique of HDX will be employed to shed more information on the chemical structures that are present.

Hydrogen-Deuterium Exchange (HDX) Experiments

The mass spectral distributions for different HDX times for the b_2, b_3, and b_4 are contrasted in Figure 3. It is found that b_2 is subject to three exchanges, while in principle having four exchangeable hydrogens. For the oxazolone N-prot and ox-prot structures, this suggests that the nitrogen-bound hydrogens are exchanged, whereas the side-chain tyrosine OH is not. Similar phenomena are also found for b_3 and b_4, which show one less exchange than the number of exchangeable hydrogens. These results are consistent with the hypothesis that the tyrosine OH is much less labile to HDX with CH_3OD. Incidentally, HDX results on the protonated amino acid tyrosine by Rožman et al. did show exchange of the phenol OH, albeit at a slow rate [48]. The absence of HDX on the phenol OH site for these b fragments supports the hypothesis that the protonated site is the "site of entry" for the deuteron, as proposed by the "relay" mechanism [49, 50]. A full deuteration of the peptide fragment would then take place via a "mobile" deuteron, which shuttles to NH amide sites on the backbone. Within this model, the deuteron does not exchange for the tyrosine OH and, hence, HDX is primarily sensitive to the chemical structure of the peptide fragment (i.e., sites of proton attachment).

Similarly to previous HDX studies [27, 28], bimodal distributions are observed for b_3 and b_4. On the other hand, b_2 solely displays one distribution. These results are consistent with the findings from IR-MPD above; where b_2 is exclusively composed of oxazolones, whereas b_4 is made up of a mixture of oxazolone and macrocycle structures. A detailed kinetic fitting of this data is given below to derive relative abundances for these structures.

Kinetic Fitting of HDX Data

To determine pseudo-first-order HDX kinetics, the natural logarithm of the relative depletion of the undeuterated peak, $\ln[d_0/\Sigma d_n]$, is plotted against the HDX time. These data are presented in Figure 4 for b_2, b_3, and b_4. Whereas a single kinetic rate (k = 0.43 s^{-1}) is observed for b_2, two distinct kinetic rates are required to fit the data for b_3 and b_4. The relative contributions of these "fast"- and "slow"-exchanging populations can be approximated by assuming that the "fast"-exchanging population is fully depleted at longer times. This implies that the rate of the "slow"-exchanging population

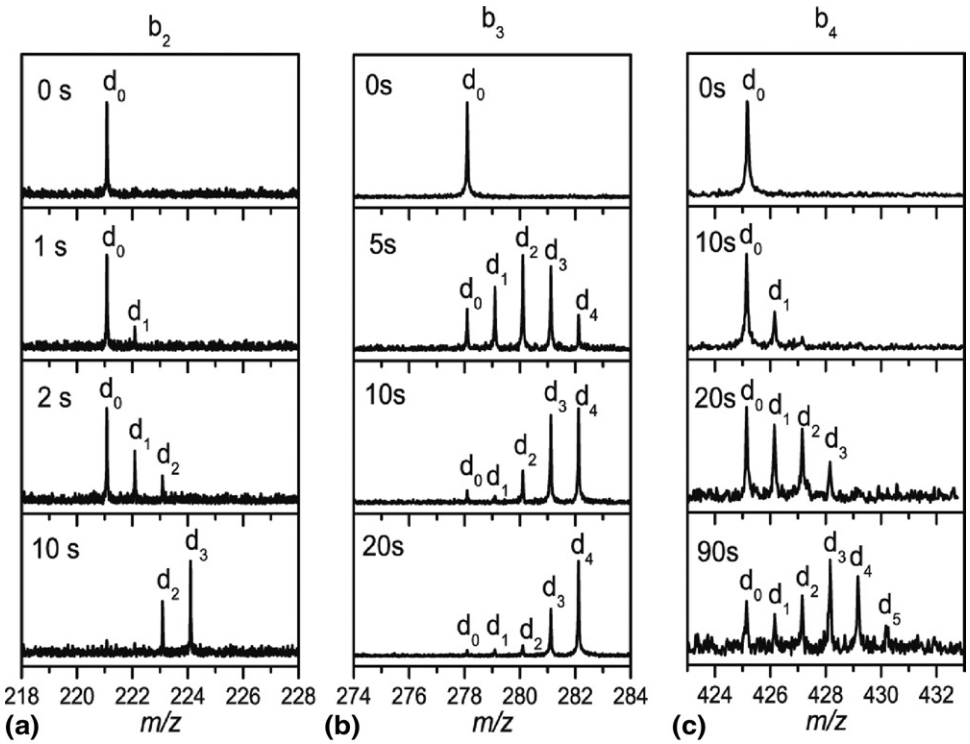

Figure 3. H/D exchange (10^{-8} Torr CH_3OD) mass spectra for (**a**) b_2, (**b**) b_3, and (**c**) b_4 for different exchange times.

can be determined accurately. A least-squares linear regression fit is employed to determine both the pseudo-first-order rate constant and the intercept. As recently shown by our group [26], the depletion of d_0 can be more conveniently represented as remaining d_0 (%) on a natural logarithm scale. The advantage of this approach is that the intercept of the "slow"-exchanging linear regression fit directly yields the relative abundance of the "slow"-exchanging structure at time zero as a percentage.

The rates and abundances from the HDX kinetic fitting results are summarized in Table 1 (detailed fitting data are shown in Table S3 in the Supporting Information). In the case of b_3, the intercept equates to a relative abundance of ~6% for the "slow"-exchanging structure at the beginning of the experiment. Note that the large error bars in this case (±34%) are due to the low ion abundance for b_3. This implies that the "fast"-exchanging structure accounts for the remainder (i.e., 94%). Note also that the higher rate at shorter HDX times in Figure 4 corresponds to the combined depletion rates of the "fast"- and "slow"-exchanging structures. Both "fast" and "slow" rates can be distinguished, as the difference in rate constant is more than an order of magnitude: $k_{slow} = 0.019\ s^{-1}$ versus $k_{fast} = 0.40\ s^{-1}$ ($= 0.42 - k_{slow}$). Similarly, the abundance of the "slow" structure in b_4 is approximated at ~31%, compared with 69% for the "fast" structure.

The exclusive presence of oxazolone structures for b_2 correlates well with a single HDX rate. Conversely, the presence of "fast" and "slow" rates for b_3 and b_4 suggest the presence of two distinct chemical structures. Given the unambiguous identification of the oxazolone structure for b_3, but more tenuous identification of the macrocycle, this strongly suggests that the majority "fast" structure corresponds to the oxazolone, whereas the "slow" structure is related to the macrocycle. In fact, the "fast" rate for b_2 and b_3 are nearly identical (0.43 versus 0.42), basically confirming that the "fast" structure corresponds to the oxazolone. For the "slow" structure, there is a significant increase from b_3 (6%) to b_4 (31%). This trend is also mirrored in the increase in intensity of the 1440 cm^{-1} band from b_3 to b_4. All of these results support the hypothesis that the "slow"-exchanging structure corresponds to the macrocycle, while the "fast"-exchanging structure is the oxazolone. The same trends were observed in our previous study on oligoglycine b fragments [26]. Moreover, in a recent study by Wysocki and coworkers on HA b_2, both oxazolone and diketopiperazine structures were considered [24].

Nonetheless, there are some differences between the present study and the oligoglycine b fragment study. For oligoglycine b_2-b_8, a general categorization into "fast"- and "slow"-exchanging structures could be established [26]. Such a categorization is less straightforward here, as the magnitude for k_{fast} and k_{slow} drop by a factor of ~10 from b_3 to b_4 (see Table 1). The slower kinetics for b_4 are possibly due to the bulky phenylalanine side-chain, which affects the H/D exchange as a

result of steric hindering. Conversely, for oligoglycine b fragments, no such side-chain effects are expected. Fortunately, the relative ratio in HDX rates between "fast" and "slow" remains similar upon going from b_3 to b_4, thus allowing their convenient separation in the kinetic analysis.

Another difference between both studies relates to the abundance of the "slow"-exchanging structure (i.e., macrocycle) for b_4, which appears to be considerably enhanced in Leu-enkephalin compared to pentaglycine (31% versus 9%). This difference must be related to the subtle primary structure differences between YGGF and GGGG, which shows that the primary structure affects the propensity for "head-to-tail" cyclization.

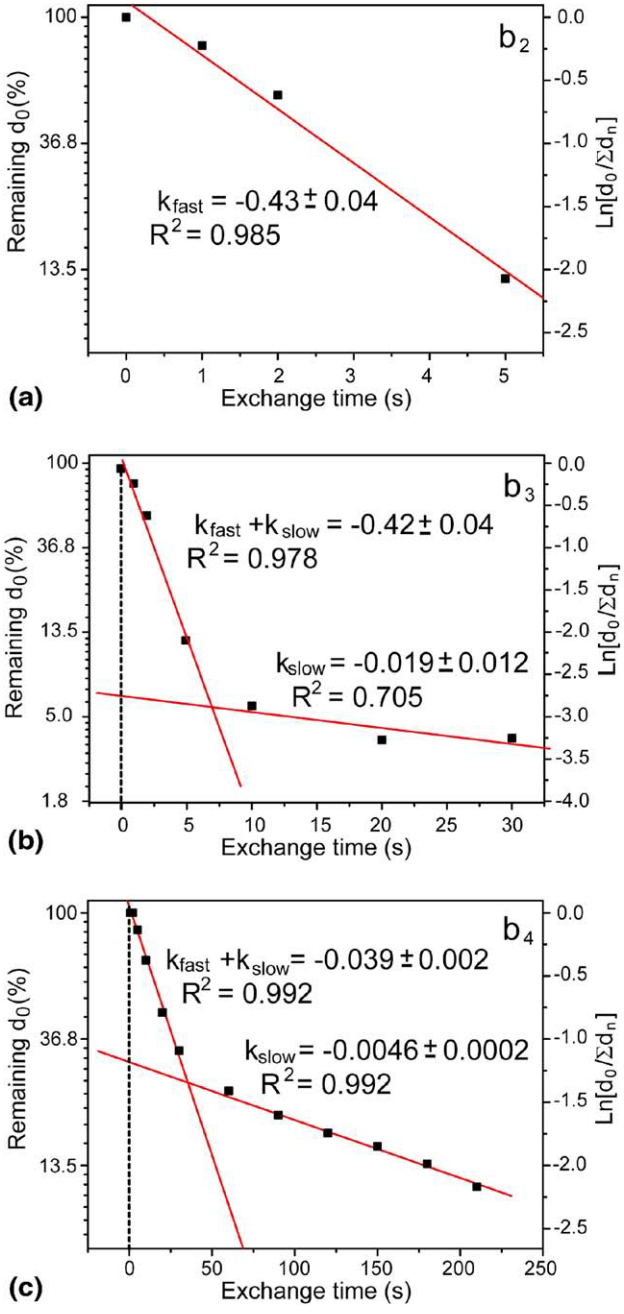

Figure 4. Kinetic fitting of the HDX results for (**a**) b_2, (**b**) b_3, and (**c**) b_4.

Table 1. Exchange rates and relative abundances of fast and slow-exchanging structures for the Leu-enkephalin fragments b_2-b_4

	Fast-exchanging structure	Slow-exchanging structure
b_2		
Rate	0.43 ± 0.04	
Abundance (%)	100	
b_3		
Rate	0.40 ± 0.04	0.019 ± 0.012
Abundance (%)	93.6 ± 34.5	6.4 ± 34.5
b_4		
Rate	0.034 ± 0.002	0.0046 ± 0.0002
Abundance (%)	69.4 ± 3.9	30.6 ± 3.9

An important realization in the comparison between the IR-MPD and HDX results for Leu-enkephalin is that the appearance of two distinct kinetics rates in the HDX experiments is only related to the presence of two considerably different chemical structures (i.e., oxazolone and macrocycle), not to the presence of different protonation sites of the same chemical structure. This suggests that the proton mobility in oxazolone structures between the N-terminal amino and C-terminal oxazolone ring N sites is faster than the kinetics of HDX. For b_2, IR-MPD measurements confirm the presence of N-prot and ox-prot oxazolones; this, however, only results in a single kinetic HDX rate. On the other hand, the presence of a mixture of oxazolone and macrocycle in b_3 and b_4 does result in the observation of two distinct HDX rates. This suggests that in the structural characterization of these b fragments, HDX is not sensitive to the site of proton attachment as such, but rather the chemical structure. This observation is consistent with the "relay" mechanism in HDX of low-basicity deuterating reagents (such as MeOD [49]). As previously discussed [26], the transition-state for HDX is likely to be higher for a macrocycle compared with an oxazolone structure, due to the ring strain in the macrocycle structure to allow this mechanism to take place.

In a recent paper in this Journal, Solouki and coworkers employed the more basic deutering reagent ND_3 to characterize b fragments, where they also distinguished "fast"- and "slow"-exchanging structures [29]. This observation is intriguing, since the mechanism of HDX for higher-basicity HDX reagents, such as ND_3, is thought to be different ('onium' mechanism, see [49]). This shows that a number of approaches are possible in the HDX characterization of b fragments, even if it remains to be seen whether the interpretation is always unambiguous.

Summary and Conclusions

In this article, we have applied IR-MPD spectroscopy (using the free electron laser FELIX) and gas-phase H/D exchange to the characterization of b_2-b_4 from

Leu-enkephalin. IR-MPD was used to qualitatively identify structures, whereas HDX was employed to quantify the structures. For b_2, by comparing the measured mid-IR spectrum (1300–1975 cm^{-1}) to theoretical spectra, the diketopiperazine structure was excluded because the prominent C=O (1810 cm^{-1}) and C–N (1715 cm^{-1}) stretches were not observed. Conversely, the characteristic oxazolone C=O stretch modes at ~1900 cm^{-1} allowed identification of N-prot and ox-prot oxazolones. The exclusive presence of one chemical structure (i.e., oxazolone) correlates well with the presence of one rate constant in the HDX measurements of b_2, which happens to be "fast". An overlay of IR-MPD spectra of b_2, b_3, and b_4 shows evidence for both macrocycle and oxazolone structures in b_3 and b_4 based on vibrations at 1440 cm^{-1} ($CO–H^+$ bending of macrocycle) and >1770 cm^{-1} (oxazolone C=O). This is in agreement with the presence of two distinct HDX rates and bimodal distributions in the corresponding HDX mass spectra. Using a recently published procedure [26] for oligoglycine b CID products, the relative abundances of the "slow"- and "fast"- exchanging structures were inferred from kinetic fitting of the HDX data. Similarly to the more extensive study on oligoglycine b_2-b_8, Leu-enkephalin b_2-b_4 show an increase in the relative abundance of the macrocycle structure with fragment size. In fact, the relative abundance for macrocycle b_4 for the sequence YGGF is considerably larger than for GGGG (31% versus 9%). This shows that apart from the chain length, the primary structure also plays a key role in the relative propensity in forming oxazolone versus macrocycle structure. While more complementary IR-MPD/HDX studies are required to validate the hypothesis that macrocycle structures exhibit slower HDX kinetics compared with oxazolones, these results show that HDX is a promising technique in quantifying both structures. In fact, HDX displays a much enhanced sensitivity relative to IR-MPD in detecting low-abundance structures, such as the macrocycle for b_3.

Acknowledgments

The authors acknowledge Dr. David Powell for the use of his Fourier transform mass spectrometer (Bruker Daltonics). The skillful assistance of the FELIX staff, in particular Dr. Britta Redlich and Dr. Lex van der Meer, is gratefully acknowledged. Travel support to The Netherlands for N.P. was provided by the NSF-PIRE (NSF-0730072). The authors thank the UF HPC Center for providing computational resources and support. N.P. thanks the University of Florida for start-up funds. This work is supported by the National Science Foundation under CHE-0845450. The American Society for Mass Spectrometry (2008 ASMS Research Award) is also acknowledged for their financial support on this project. J.D.S. and J.O. were supported by the Nederlandse Organisatie voor Wetenschappelijk Onderzoek (Dutch National Science Foundation). Construction and shipping of the FTMS instrument was made possible through funding from the National High Field FT-ICR Facility (grant CHE-9909502) at the National High Magnetic Field Laboratory, Tallahassee, FL, on the initiative of Professor John R. Eyler and Professor Alan G. Marshall.

Appendix A
Supplementary Material

Supplementary material associated with this article may be found in the online version at doi:10.1016/j.jasms.2010.02.022.

References

1. Fenn, J. B.; Mann, M.; Meng, C. K.; Wong, S. F.; Whitehouse, C. M. Electrospray Ionization for Mass Spectrometry of Large Biomolecules. *Science* **1989,** *246,* 64–71.
2. Yamashita, M.; Fenn, J. B. Electrospray Ion Source. Another Variation on the Free-Jet Theme. *J. Am. Chem. Soc.* **1984,** *88,* 4451–4459.
3. Karas, M.; Hillenkamp, F. Laser Desorption Ionization of Proteins with Molecular Masses Exceeding 10,000 Daltons. *Anal. Chem.* **1988,** *60,* 2299–2301.
4. Hillenkamp, F.; Karas, M.; Beavis, R. C.; Chait, B. T. Matrix-Assisted Laser Desorption Ionization Mass-Spectrometry of Biopolymers. *Anal. Chem.* **1991,** *63,* A1193–A1202.
5. Hillenkamp, F.; Karas, M.; Beavis, R. C.; Chait, B. T. Matrix-Assisted Laser Desorption Ionization Mass-Spectrometry of Biopolymers. *Anal. Chem.* **1991,** *63,* A1193–A1202.
6. Roepstorff, P.; Fohlmann, J. Proposal for a Common Nomenclature for Sequence Ions in the Mass Spectra of Peptides. *J. Biomed. Mass Spectrom.* **1984,** *11,* 601.
7. Biemann, K. Contributions of Mass Spectrometry to Peptide and Protein Structure. *Biomed. Environ. Mass Spectrom.* **1988,** *16,* 99–111.
8. Burlet, O.; Yang, C. Y.; Gaskell, S. J. *J. Am. Soc. Mass Spectrom.* **1992,** *3,* 337–344.
9. Dongre, A. R.; Jones, J. L.; Somogyi, A.; Wysocki, V. H. Influence of Peptide Composition, Gas-Phase Basicity, and Chemical Modification on Fragmentation Efficiency: Evidence for the Mobile Proton Model. *J. Am. Chem. Soc.* **1996,** *118,* 8365–8374.
10. Wysocki, V. H.; Tsaprailis, G.; Smith, L. L.; Breci, L. A. Mobile and Localized Protons: A Framework for Understanding Peptide Dissociation. *J. Mass Spectrom.* **2000,** *35,* 1399–1406.
11. Harrison, A. G. To b or Not to b: The Ongoing Saga of Peptide b Ions. *Mass Spectrom. Rev.* **2009,** *28,* 640–654.
12. Yalcin, T.; Khouw, C.; Csizmadia, I. G.; Peterson, M. R.; Harrison, A. G. Why are b Ions Stable Species in Peptide Spectra? *J. Am. Soc. Mass Spectrom.* **1995,** *6,* 1165–1174.
13. Farrugia, J.; O'Hair, R. A. J.; Reid, G. Do All b_2 Ions Have Oxazolone Structures? Multistage Mass Spectrometry and Ab Initio Studies on Protonated N-Acyl Amino Acid Methyl Ester Model Systems. *Int. J. Mass Spectrom.* **2001,** *210/211,* 71–87.
14. Farrugia, J.; O'Hair, R. A. J. Involvement of Salt Bridges in a Novel Gas Phase Rearrangement of Protonated Arginine-Containing Dipeptides, which precedes fragmentation. *Int. J. Mass Spectrom.* **2003,** *222,* 229–242.
15. Huang, Y.; Wysocki, V. H.; Tabb, D. L.; Yates, J. R. The Influence of Histidine on Cleavage C-Terminal to Acidic Residues in Doubly Protonated Tryptic Peptides. *Int. J. Mass Spectrom.* **2002,** *219,* 233–244.
16. Kish, M. M.; Wesdemiotis, C. Selective Cleavage at Internal Lysine Residues in Protonated Versus Metalated Peptides. *Int. J. Mass Spectrom.* **2003,** *227,* 191–201.
17. Harrison, A. G.; Young, A. B.; Bleiholder, B.; Suhai, S.; Paizs, B. Scrambling of Sequence Information in Collision-Induced Dissociation of Peptides. *J. Am. Chem. Soc.* **2006,** *128,* 10364–10365.
18. Tang, X.; Thibault, P.; Boyd, R. K. Fragmentation Reactions of Multiply-Protonated Peptides and Implications for Sequencing by Tandem Mass-Spectrometry with Low-Energy Collision-Induced Dissociation. *Anal. Chem.* **1993,** *65,* 2824–2834.
19. Tang, X.; Boyd, R. K. Rearrangement of Doubly-Charged Acylium Ions from Lysyl and Ornithyl Peptides. *Rapid Commun. Mass Spectrom.* **1994,** *8,* 678–686.
20. Vachet, R. W.; Bishop, B. M.; Erickson, B. W.; Glish, G. L. Novel Peptide Dissociation: Gas-Phase Intramolecular Rearrangement of Internal Amino Acid Residues. *J. Am. Chem. Soc.* **1997,** *119,* 5481–5488.
21. Polfer, N. C.; Oomens, J.; Suhai, S.; Paizs, B. Infrared Spectroscopy and Theoretical Studies on Gas-Phase Protonated Leu-Enkephalin and Its Fragments: Direct Evidence for the Mobile Proton. *J. Am. Chem. Soc.* **2007,** *129,* 5887–5897.
22. Yoon, S.; Chamot-Rooke, J.; Perkins, B.; Hilderbrand, A. E.; Poutsma, J.; Wysocki, V. H. IRMPD Spectroscopy Shows that AGG Forms an Oxazolone b Ion. *J. Am. Chem. Soc.* **2008,** *130,* 17644–17645.
23. Oomens, J.; Young, S.; Molesworth, S.; van Stipdonk, M. J. Spectroscopic Evidence for an Oxazolone Structure of the b2 Fragment Ion from Protonated Tri-Alanine. *J. Am. Soc. Mass Spectrom.* **2009,** *20,* 334–339.
24. Perkins, B.; Chamot-Rooke, J.; Yoon, S.; Gucinski, A.; Somogyi, A.; Wysocki, V. H. Evidence of Diketopiperazine and Oxazolone Structures for HA b2+ Ion. *J. Am. Chem. Soc.* **2009,** *131,* 17528–17529.
25. Bythell, B.; Erlekam, U.; Paizs, B.; Maitre, P. Infrared Spectroscopy of Fragments from Doubly Protonated Tryptic Peptides. *Chem. Phys. Chem.* **2009,** *10,* 883–885.

26. Chen, X.; Yu, L.; Steill, J. D.; Oomens, J.; Polfer, N. Effect of Peptide Fragment Size on the Propensity of Cyclization in Collision-Induced Dissociation: Oligoglycine b2-b8. *J. Am. Chem. Soc.* **2009,** *131,* 18272–18282.
27. Herrmann, K. A.; Kuppannan, K.; Wysocki, V. H. Fragmentation of Doubly-Protonated Peptide Ion Populations Labeled by H/D Exchange with CH_3OD. *Int. J. Mass Spectrom.* **2006,** *249/250,* 93–105.
28. Somogyi, A. Probing Peptide Fragment Ion Structures by Combining Sustained Off-Resonance Collision-Induced Dissociation and Gas-Phase H/D Exchange (SORI-HDX) in Fourier Transform Ion-Cyclotron Resonance (FT-ICR) Instruments. *J. Am. Soc. Mass Spectrom.* **2008,** *19,* 1771–1775.
29. Fattahia, A.; Zekavata, B.; Solouki, T. H/D Exchange Kinetics: Experimental Evidence for Formation of Different b Fragment Ion Conformers/Isomers During the Gas-Phase Peptide Sequencing. *J. Am. Soc. Mass Spectrom.* **2009,** *21,* 358–369.
30. Garcia, I.; Giles, K.; Bateman, R. H.; Gaskell, S. J. Studies of Peptide a- and b-Type Fragment Ions Using Stable Isotope Labeling and Integrated Ion Mobility/Tandem Mass Spectrometry. *J. Am. Soc. Mass Spectrom.* **2008,** *19,* 1781–1787.
31. Garcia, I.; Giles, K.; Bateman, R. H.; Gaskell, S. J. Evidence for Structural Variants of a- and b-Type Peptide Fragment Ions Using Combined Ion Mobility/Mass Spectrometry. *J. Am. Soc. Mass Spectrom.* **2008,** *19,* 609–613.
32. Polfer, N. C.; Bohrer, B. C.; Plasencia, M. D.; Paizs, B.; Clemmer, D. E. On the Dynamics of Fragment Isomerization in Collision-Induced Dissociation of Peptides. *J. Phys. Chem. A* **2008,** *112,* 1286–1293.
33. Oepts, D.; van der Meer, A. F. G.; van Amersfoort, P. W. The Free-Electron-Laser User Facility FELIX. *Infrared Phys. Technol.* **1995,** *36,* 297–308.
34. Valle, J. J.; Eyler, J. R.; Oomens, J.; Moore, D. T.; van der Meer, A. F. G.; von Helden, G.; Meijer, G.; Hendrickson, C. L.; Marshall, A. G.; Blakney, G. T. A Free Electron-Fourier Transform Ion Cyclotron Resonance Mass Spectrometry Facility for Obtaining Infrared Multiphoton Dissociation Spectra of Gaseous Ions. *Rev. Sci. Instrum.* **2005,** *76,* 23103.
35. Polfer, N. C.; Oomens, J.; Moore, D. T.; von Helden, G.; Meijer, G.; Dunbar, R. C. Infrared Spectroscopy of Phenylalanine Ag(I) and Zn(II) Complexes in the Gas Phase. *J. Am. Chem. Soc.* **2006,** *128,* 517–525.
36. Dopfer, O. IR Spectroscopy of Microsolvated Aromatic Cluster Ions: Ionization-Induced Switch in Aromatic Molecule-Solvent Recognition. *Z Phys. Chem.* **2005,** *219,* 125–168.
37. Oomens, J.; Sartakov, B.; Meijer, G.; von Helden, G. Gas-Phase Infrared Multiple Photon Dissociation Spectroscopy of Mass-Selected Molecular Ions. *Int. J. Mass Spectrom.* **2006,** *254,* 1–19.
38. Polfer, N. C.; Oomens, J. Reaction Products in Mass Spectrometry Elucidated with Infrared Spectroscopy. *Phys. Chem., Chem. Phys.* **2007,** *9,* 3804–3817.
39. Asmis, K. R.; Sauer, J. Mass-Selective Vibrational Spectroscopy of Vanadium Oxide Cluster Ions. *Mass Spectrom. Rev.* **2007,** *26,* 542–562.
40. MacAleese, L.; Maitre, P. Infrared Spectroscopy of Organometallic Ions in the Gas Phase: From Model to Real World Complexes. *Mass Spectrom. Rev.* **2007,** *26,* 583–605.
41. Eyler, J. R. Infrared Multiple Photon Dissociation Spectroscopy of Ions in Penning Traps. *Mass Spectrom. Rev.* **2009,** *28,* 448–467.
42. Polfer, N. C.; Oomens, J. Vibrational Spectroscopy of Bare and Solvated Ionic Complexes of Biological Relevance. *Mass Spectrom. Rev.* **2009,** *28,* 468–494.
43. Fridgen, T. D. Infrared Consequence Spectroscopy of Protonated and Metal Ion Cationized Complexes. *Mass Spectrom. Rev.* **2009,** *28,* 586–607.
44. Cornell, W. D.; Cieplak, P.; Bayly, C. I.; Gould, I. R.; Merz, K.; M.; Ferguson, D. M.; Spellmeyer, D. C.; Fox, T.; Caldwell, J. W.; Kollmann, P. A. A Second Generation Force Field for the Simulation of Proteins, Nucleic Acids, and Organic Molecules. *J. Am. Chem. Soc.* **1995,** *117,* 5179–5197.
45. Frisch, M. J.; Trucks, G. W.; Schlegel, H. B.; Scuseria, G. E.; Robb, M. A.; Cheeseman, J. R.; Montgomery, J. A. Jr.; Vreven, T.; Kudin, K. N.; Burant, J. C.; Millam, J. M.; Iyengar, S. S.; Tomasi, J.; Barone, V.; Mennucci, B.; Cossi, M.; Scalmani, G.; Rega, N.; Petersson, G. A.; Nakatsuji, H.; Hada, M.; Ehara, M.; Toyota, K.; Fukuda, R.; Hasegawa, J.; Ishida, M.; Nakajima, T.; Honda, Y.; Kitao, O.; Nakai, H.; Klene, M.; Li, X.; Knox, J. E.; Hratchian, H. P.; Cross, J. B.; Bakken, V.; Adamo, C.; Jaramillo, J.; Gomperts, R.; Stratmann, R. E.; Yazyev, O.; Austin, A. J.; Cammi, R.; Pomelli, C.; Ochterski, J. W.; Ayala, P. Y.; Morokuma, K.; Voth, G. A.; Salvador, P.; Dannenberg, J. J.; Zakrzewski, V. G.; Dapprich, S.; Daniels, A. D.; Strain, M. C.; Farkas, O.; Malick, D. K.; Rabuck, A. D.; Raghavachari, K.; Foresman, J. B.; Ortiz, J. V.; Cui, Q.; Baboul, A. G.; Clifford, S.; Cioslowski, J.; Stefanov, B. B.; Liu, G.; Liashenko, A.; Piskorz, P.; Komaromi, I.; Martin, R. L.; Fox, D. J.; Keith, T.; Al-Laham, M. A.; Peng, C. Y.; Nanayakkara, A.; Challacombe, M.; Gill, P. M. W.; Johnson, B.; Chen, W.; Wong, M. W.; Gonzalez, C.; Pople, J. A. *Gaussian 03*, Revision C 02; Gaussian, Inc.; Wallingford, CT, 2004.
46. Cieplak, P.; Cornell, W. D.; Bayly, C. I.; Kollmann, P. A. Application for the Multimolecule and Multiconformational RESP Methodology to Biopolymers: Charge Derivation for DNA, RNA, and Proteins. *Comput. Chem.* **1995,** *16,* 1357–1377.
47. Paizs, B.; Suhai, S. Towards Understanding the Tandem Mass Spectra of Protonated Oligopeptides. 1: Mechanism of Amide Bond Cleavage. *J. Am. Soc. Mass Spectrom.* **2004,** *15,* 103–113.
48. Rožman, M.; Kazazic, S.; Klasinc, L.; Sric, D. Kinetics of Gas-Phase Hydrogen/Deuterium Exchange and Gas-Phase Structure of Protonated Phenylalanine, Proline, Tyrosine, and Tryptophan. *Rapid Commun. Mass Spectrom.* **2003,** *17,* 2769–2772.
49. Campbell, S.; Rodgers, M. T.; Marzluff, E. M.; Beauchamp, J. L. Deuterium Exchange Reactions as Probe of Biomolecule Structure. Fundamental Studies of Gas Phase Reactions of Protonated Glycine Oligomers with D_2O, CD_3OD, CD_3CO_2D, and ND_3. *J. Am. Chem. Soc.* **1995,** *117,* 12840–12854.
50. Wyttenbach, T.; Bowers, M. T. Gas Phase Conformations of Biological Molecules: The Hydrogen/Deuterium Exchange Mechanism. *J. Am. Soc. Mass Spectrom.* **1999,** *10,* 9–14.